


 Cite this: *RSC Adv.*, 2023, **13**, 19617

## Ultrasound-assisted degradation of organophosphorus pesticide methidathion using $\text{CuFe}_2\text{O}_4@\text{SiO}_2\text{-GO}_{\text{COOH}}$ as a magnetic separable sonocatalyst

Houda Maati,<sup>\*ab</sup> Othmane Amadine,<sup>ID \*ab</sup> Younes Essamlali,<sup>ab</sup> Soumia Aboulhrouz,<sup>ID ab</sup> Ilham jioui,<sup>ab</sup> Karim Dânoun<sup>ab</sup> and Mohamed Zahouily<sup>\*abc</sup>

Water contamination by pesticides is a critical environmental issue, necessitating the development of sustainable and efficient degradation methods. This study focuses on synthesizing and evaluating a novel heterogeneous sonocatalyst for degrading pesticide methidathion. The catalyst consists of graphene oxide (GO) decorated  $\text{CuFe}_2\text{O}_4@\text{SiO}_2$  nanocomposites. Comprehensive characterization using various techniques confirmed the superior sonocatalytic activity of the  $\text{CuFe}_2\text{O}_4@\text{SiO}_2\text{-GO}_{\text{COOH}}$  nanocomposite compared to  $\text{CuFe}_2\text{O}_4@\text{SiO}_2$  alone. The enhanced performance is attributed to the combined effects of GO and  $\text{CuFe}_2\text{O}_4@\text{SiO}_2$ , including increased surface area, enhanced adsorption capabilities, and efficient electron transfer pathways. Reaction parameters such as time, temperature, concentration, and pH significantly influenced the degradation efficiency of methidathion. Longer reaction times, higher temperatures, and lower initial pesticide concentrations favored faster degradation and higher efficiency. Optimal pH conditions were identified to ensure effective degradation. Remarkably, the catalyst demonstrated excellent recyclability, indicating its potential for practical implementation in pesticide-contaminated wastewater treatment. This research contributes to the development of sustainable methods for environmental remediation, highlighting the promising potential of the graphene oxide decorated  $\text{CuFe}_2\text{O}_4@\text{SiO}_2$  nanocomposite as an effective heterogeneous sonocatalyst for pesticide degradation.

Received 26th April 2023  
 Accepted 14th June 2023

DOI: 10.1039/d3ra02773b  
[rsc.li/rsc-advances](http://rsc.li/rsc-advances)

### 1. Introduction

For more than two decades, pesticides have been extensively employed in various sectors, including agriculture, road maintenance, rail infrastructure, wood treatment, and even for private use such as gardening and premises treatment.<sup>1</sup> While they aid in controlling pests, they also pose a significant threat to water pollution. Pesticide use has been steadily increasing over the past six decades, with tonnages reaching alarming levels.<sup>2</sup> Pesticides are not only a concern for applicators who are most exposed to them, but also for the general population due to the real public health problem they pose.<sup>3,4</sup> The body absorbs pesticides, particularly by ingestion, through the skin, and by the respiratory tract.<sup>5</sup> Furthermore, epidemiological studies have demonstrated that individuals who frequently use pesticides without protection are more likely to develop certain

illnesses such as cancer, birth defects, sterility, neurological disorders, or weakened immune systems.<sup>6</sup> Pesticide residues are ubiquitous, found not only in water but also in air, mist, soil, food, and even in the blood.<sup>7,8</sup>

Pesticides are a major cause of water contamination.<sup>9,10</sup> When they are spread over soil, they can infiltrate and contaminate groundwater.<sup>11</sup> This contamination can affect water quality and lead to the need for additional treatments.<sup>12</sup> The majority of pesticides found in rivers and groundwater are herbicides,<sup>13,14</sup> which are used to kill weeds in agricultural and non-agricultural areas.

To protect the environment, it is essential to treat urban, industrial, and agricultural wastewater. Various methods are currently available and well-controlled on a laboratory scale, which can be applied on a large scale. These methods include membrane technologies, adsorption techniques, ion exchange, and solid-liquid separation processes.<sup>15–18</sup> However, these processes are only separative, not degradative, and have several disadvantages, such as producing pollutant concentrates, sludge, and requiring significant consumption of chemical reagents. Biological purification processes are commonly used for treating polluted waters,<sup>19</sup> but this process generates large

<sup>a</sup>Moroccan Foundation for Advanced Science, Innovation and Research (MASCIR), Benguerir, Morocco. E-mail: [m.zahouily@mascir.com](mailto:m.zahouily@mascir.com); [o.amadine@mascir.com](mailto:o.amadine@mascir.com)

<sup>b</sup>Mohammed VI Polytechnic University, Lot 660 – Hay Moulay Rachid, Ben Guerir, 43150, Morocco

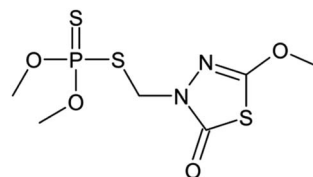
<sup>c</sup>Laboratory of Materials, Catalysis & Valorization of Natural Resources, Hassan II University, FST-Mohammedia, Morocco



quantities of biological sludge that must be treated. Additionally, these methods may not be applicable to effluents with a high concentration of pollutants. Therefore, it is necessary to use more reactive systems than those adopted in conventional purification processes.

To address this problem, advanced oxidation processes (AOPs) have been developed and are increasingly being used.<sup>20,21</sup> These methods involve the formation of hydroxyl radicals ( $\text{HO}^\cdot$ ), which are highly reactive chemicals that break down pollutants into biologically degradable molecules or mineral compounds, such as  $\text{CO}_2$  and  $\text{H}_2\text{O}$ .<sup>22</sup> Because hydroxyl radicals are very reactive and unstable,<sup>23</sup> they must be continuously produced through various means, including chemical, photochemical, biological, or electrochemical methods.<sup>24</sup> Among these processes, we are particularly interested in sonolysis for the degradation of organic pollutants.<sup>25</sup> Ultrasound waves are propagated in the solution to be treated, but using ultrasound alone for pollutant degradation requires high energy and long reaction times.<sup>26,27</sup> To overcome these problems, low-power ultrasonic irradiation has been combined with heterogeneous catalysis to create a sonocatalytic system,<sup>28-30</sup> which can increase the rate of pollutant degradation and reduce reaction times. Various materials have been used as sonocatalysts for organic pollutant degradation, including Rutile  $\text{TiO}_2$ ,<sup>31</sup>  $\text{ZnO}$ /biochar,<sup>32</sup>  $\text{TiO}_2/\text{ZnO}$ ,<sup>33</sup>  $\text{Zr}/\text{TiO}_2$ ,<sup>34</sup>  $\text{SiO}_2$ ,<sup>35</sup>  $\text{CuO}$ .<sup>36</sup> Among the various heterogeneous catalysts, magnetic materials have caught the attention of the industrial community because they are less expensive, readily available, recyclable, and exhibit significant improvement due to their high surface area, small particle size, and high active sites.<sup>37</sup> Additionally, these magnetic nanoparticles can be efficiently separated after completion of the reaction by a simple external magnet, which is advantageous compared to classical techniques such as centrifugation and filtration. In particular, the spinel  $\text{CuFe}_2\text{O}_4$ , a magnetic material, has gained intensive attention due to its high catalytic activity and ease of separation from the reaction system.<sup>38</sup> However, the traditional methods used for the preparation of  $\text{CuFe}_2\text{O}_4$  produce aggregated particles that influence their catalytic properties.<sup>39</sup> To overcome this problem, different approaches have been developed. Among them, coating  $\text{CuFe}_2\text{O}_4$  with silica has been found to be an effective approach to reduce the tendency of particle agglomeration.<sup>40</sup> Furthermore, silanol groups presented on the surface of silica offer the possibility for the immobilization of a variety of functionalized materials that can improve the catalytic activity of  $\text{CuFe}_2\text{O}_4$ .<sup>41,42</sup> Graphene oxide (GO) is a promising candidate for the immobilization of  $\text{CuFe}_2\text{O}_4$  materials, as it can improve the degradation rate of organic pollutants through an increase in the production of hydroxyl radicals ( $\text{HO}^\cdot$ ) from the functional groups on the surface of GO.<sup>43,44</sup>

In this study, a  $\text{CuFe}_2\text{O}_4@\text{SiO}_2$  material decorated with graphene oxide (GO) was synthesized using a simple and efficient method. The physical and chemical properties of the samples were characterized through various techniques including nitrogen adsorption-desorption, scanning electron microscopy (SEM), X-ray diffraction (XRD), and Fourier transform infrared spectroscopy (FTIR). The performance of the magnetic material  $\text{CuFe}_2\text{O}_4@\text{SiO}_2\text{-GO}_{\text{COOH}}$  as a sonocatalytic system for degrading organic pollutants was evaluated, with methidathion pesticide



Scheme 1 Structure of methidathion pesticide.

(Scheme 1) selected as the target pollutant. Optimization of reaction parameters such as reaction kinetics, temperature, methidathion concentration, and pH was conducted. Furthermore, the reusability of the  $\text{CuFe}_2\text{O}_4@\text{SiO}_2\text{-GO}_{\text{COOH}}$  sonocatalytic system was investigated.

## 2. Experimental

### 2.1 Chemical reagents

Methidathion pesticide ( $\text{C}_6\text{H}_{11}\text{N}_2\text{O}_4\text{PS}_3$ ), hydrogen peroxide  $\text{H}_2\text{O}_2$  (30% w/w), iron chloride hexahydrate ( $\text{FeCl}_3 \cdot 6\text{H}_2\text{O}$ ), copper nitrate ( $\text{Cu}(\text{NO}_3)_2 \cdot 3\text{H}_2\text{O}$ ), polyvinylpyrrolidone (PVP), sodium hydroxide (NaOH), graphite, sodium nitrate ( $\text{NaNO}_3$ ), sulfuric acid ( $\text{H}_2\text{SO}_4$ ) (98% w/w), tetra-ethyl-*ortho*-silicate (TEOS), sodium acetate anhydrous (NaAc) 3-(trimethoxysilyl) propylamine (APTMS), ethylene glycol (EG) and potassium permanganate ( $\text{KMnO}_4$ ) were purchased from Aldrich chemical company. All the reagents were used without further purification. Water used in all experiments was deionized.

### 2.2 Materials preparation

**2.2.1 Preparation of  $\text{CuFe}_2\text{O}_4$ .**  $\text{CuFe}_2\text{O}_4$  nanoparticles were synthesized using a hydrothermal method.<sup>45</sup> In the typical procedure, 1 g of polyvinylpyrrolidone (PVP) was dissolved in 40 mL of ethylene glycol, and the solution was stirred until it became clear. Then,  $\text{Cu}(\text{NO}_3)_2 \cdot 3\text{H}_2\text{O}$  (2.5 mmol),  $\text{FeCl}_3 \cdot 6\text{H}_2\text{O}$  (5 mmol), and NaAc (30 mmol) were added to the solution with continuous stirring. The molar ratio of  $\text{Cu}^{2+}$  to  $\text{Fe}^{3+}$  was maintained at 1 : 2. The mixture was stirred vigorously for 60 min and then transferred to a 50 mL Teflon-lined stainless-steel autoclave, which was sealed and heated at 200 °C for 8 h. The resulting brown product was collected using an external magnetic field, washed several times with ethanol and deionized water, and then dried at 80 °C for 1 h in a hot vacuum desiccator.

**2.2.2 Preparation of  $\text{CuFe}_2\text{O}_4@\text{SiO}_2\text{-NH}_2$ .**  $\text{CuFe}_2\text{O}_4@\text{SiO}_2\text{-NH}_2$  nanoparticles were synthesized according to Lieu *et al.*<sup>46</sup> with a few modifications. Initially, a mixture of 2-propanol (50 mL) and water (12.8 mL) was utilized to disperse 500 mg of  $\text{CuFe}_2\text{O}_4$  nanoparticles using ultrasonic irradiation. Following that, 10 mL of ammonium hydroxide and 4 mL of tetra-ethyl-*ortho*-silicate (TEOS) were added to the dispersion. The resulting mixture was stirred at room temperature for 10 hours. The product was subsequently collected using an external magnet, washed multiple times with water and ethanol, and dried at 60 °C. The resulting magnetic  $\text{CuFe}_2\text{O}_4@\text{SiO}_2$  nanoparticles were then dispersed in 50 mL of toluene. To introduce amino



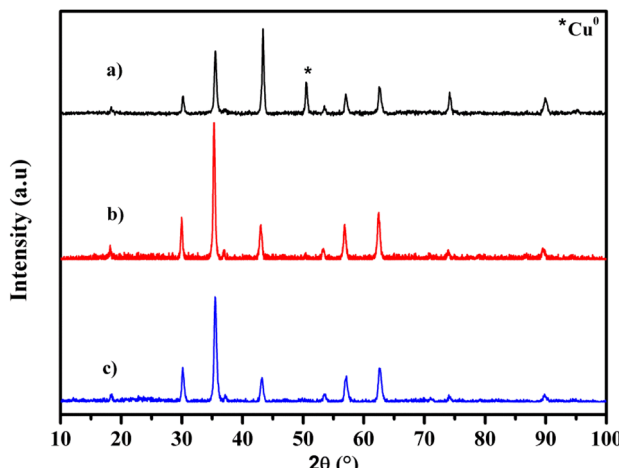


Fig. 1 XRD patterns of  $\text{CuFe}_2\text{O}_4$  (a),  $\text{CuFe}_2\text{O}_4@\text{SiO}_2$  (b) and  $\text{CuFe}_2\text{O}_4@\text{SiO}_2\text{-GO}_{\text{COOH}}$  (c).

functionality, 4.0 mL of 3-(trimethoxysilyl)propylamine (APTMS) was added to the solution. The mixture was refluxed for 10 hours under a nitrogen atmosphere.

**2.2.3 Preparation of  $\text{CuFe}_2\text{O}_4@\text{SiO}_2\text{-GO}_{\text{COOH}}$ .** Firstly, graphene oxide (GO) was synthesized from natural graphite using the modified Hummers' method.<sup>47</sup> Next, 2 g of NaOH and 2 g of  $\text{ClCH}_2\text{COOH}$  were added to a suspension of GO (35 mg in 100 mL of deionized water) and sonicated for 2 hours to convert the OH groups of GO into COOH groups. The resulting product was neutralized using diluted hydrochloric acid and then purified through repeated rinsing and centrifugation until it was well dispersed in distilled water. The GO-COOH suspension was then dialyzed against distilled water for over 72 hours to remove any ions. Finally, the  $\text{CuFe}_2\text{O}_4@\text{SiO}_2\text{-GO}_{\text{COOH}}$  product was obtained *via* covalent bonding between the carboxylic groups of GO and the amine groups of  $\text{CuFe}_2\text{O}_4@\text{SiO}_2\text{-NH}_2$ . In a typical synthesis, 10 mg of GO-COOH was dispersed in 20 mL of deionized water for 3 hours, followed by the addition of 10 mg  $\text{CuFe}_2\text{O}_4@\text{SiO}_2\text{-NH}_2$  under continuous stirring for 24 hours at room temperature. The resulting product,  $\text{CuFe}_2\text{O}_4@\text{SiO}_2\text{-GO}_{\text{COOH}}$ , was collected using an external magnetic field, washed several times with ethanol and deionized water, and then dried at 60 °C for 1 hour in a hot vacuum desiccator.

### 2.3 Characterization

X-ray diffraction (XRD) measurements were conducted using Cu-K $\alpha$  radiation in Bragg–Brentano geometry ( $2\theta$ ) on a Bruker AXS D-8 diffractometer. Fourier transform infrared

spectroscopy (FTIR) was performed on all samples in the range of 4000–400  $\text{cm}^{-1}$ , using an ABB Bomem FTLA 2000 spectrometer with a 16  $\text{cm}^{-1}$  resolution. Scanning electron microscopy (SEM) and scanning transmission electron microscopy (STEM) micrographs were obtained using a Tecnai G2 microscope at 120 kV. The elemental composition of the  $\text{CuFe}_2\text{O}_4@\text{SiO}_2\text{-GO}_{\text{COOH}}$  nanocomposite was confirmed by energy dispersive X-ray analysis (EDX). The magnetic properties of  $\text{CuFe}_2\text{O}_4$  nanoparticles and the  $\text{CuFe}_2\text{O}_4@\text{SiO}_2\text{-GO}_{\text{COOH}}$  nanocomposite were investigated using a MPMS-XL-7AC superconducting quantum interference device (SQUID) magnetometer. Magnetic measurements were performed at room temperature from –15 000 to 15 000 Oe. Zeta potential measurements were carried out using a Zetasizer Nano Series (ZS90).

### 2.4 Catalytic test procedure

The sonocatalytic degradation of methidathion was carried out using the  $\text{CuFe}_2\text{O}_4@\text{SiO}_2\text{-GO}_{\text{COOH}}$  catalyst in the presence of  $\text{H}_2\text{O}_2$ . The catalytic test was carried out in triplicate to obtain the mean value. The reaction was performed in a 50 mL beaker for 60 minutes. Sonication was carried out in an ultrasonic cleaning bath (ELMAS60H) operating at 37 kHz and a power of 600 W. A water-circulating unit was used to control the water bath temperature. In a typical procedure, 25 mL of  $\text{H}_2\text{O}_2$  was added to the methidathion solution under ultrasound irradiation. Subsequently, 10 mg of the catalyst was added to initiate

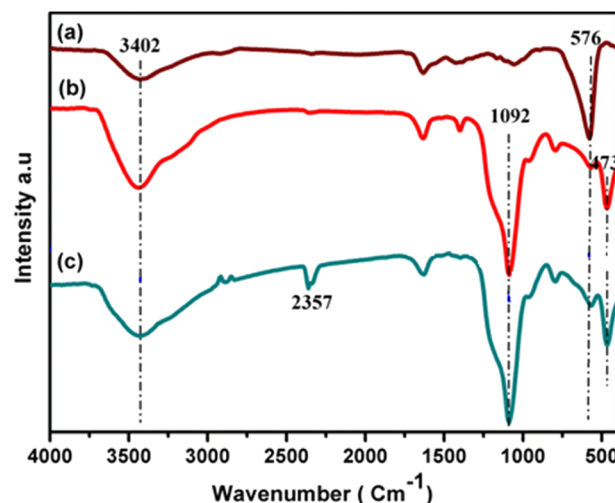


Fig. 2 FT-IR spectra of  $\text{CuFe}_2\text{O}_4$  (a),  $\text{CuFe}_2\text{O}_4@\text{SiO}_2$  (b), and  $\text{CuFe}_2\text{O}_4@\text{SiO}_2\text{-GO}_{\text{COOH}}$  (c).

Table 1 Lattice parameter, crystallite size of  $\text{CuFe}_2\text{O}_4$ ,  $\text{CuFe}_2\text{O}_4@\text{SiO}_2$  and  $\text{CuFe}_2\text{O}_4\text{-SiO}_2\text{-GO}_{\text{COOH}}$  samples

Samples	Lattice parameter $a$ ( $\text{\AA}$ )	Cell volume ( $\text{\AA}^3$ )	Crystallite size (nm)
$\text{CuFe}_2\text{O}_4$	8.3783	588.1182	21.8
$\text{CuFe}_2\text{O}_4@\text{SiO}_2$	8.4140	595.6643	22.4
$\text{CuFe}_2\text{O}_4@\text{SiO}_2\text{-GO}_{\text{COOH}}$	8.3799	588.4558	19.8



the reaction. At specific time intervals, a predetermined volume (2.0 mL) of the reaction mixture was withdrawn and filtered using a micro-filter (45 mm) to remove the solid catalyst. The concentration of methidathion was determined using high-performance liquid chromatography (HPLC Shimadzu Kyoto, Japan) equipped with a reversed-phase C18 column (150 mm  $\times$  4.6 mm  $\times$  5  $\mu\text{m}$ ) using methanol/water ((40/60) volume ratio) as the mobile phase at a flow rate of 0.5 mL min $^{-1}$  with UV detection.

### 3. Results and discussion

The crystalline structure of CuFe<sub>2</sub>O<sub>4</sub>, CuFe<sub>2</sub>O<sub>4</sub>@SiO<sub>2</sub> and CuFe<sub>2</sub>O<sub>4</sub>@SiO<sub>2</sub>-GO<sub>COOH</sub> was investigated by X-ray diffraction (XRD). As shown in Fig. 1, the diffraction peaks located at 30.1°,

35.5°, 43.1°, 57.0°, and 62.9°, which correspond to the crystal planes of (202), (311), (004), (333), and (440), respectively, can be readily attributed to the tetragonal-type CuFe<sub>2</sub>O<sub>4</sub> (JCPDS 34-0425).<sup>48</sup> However, we observed the presence of an XRD peak of metallic copper in the CuFe<sub>2</sub>O<sub>4</sub> sample, which can be explained by the reduction of copper in the presence of ethylene glycol.<sup>49</sup> Similar peaks characteristic of CuFe<sub>2</sub>O<sub>4</sub> were also detected in the case of CuFe<sub>2</sub>O<sub>4</sub>@SiO<sub>2</sub> and CuFe<sub>2</sub>O<sub>4</sub>@SiO<sub>2</sub>-GO<sub>COOH</sub>, indicating the stability of our materials after silica coating. Furthermore, we observed the disappearance of metallic copper diffraction peaks in CuFe<sub>2</sub>O<sub>4</sub>@SiO<sub>2</sub>, CuFe<sub>2</sub>O<sub>4</sub>@SiO<sub>2</sub>-GO<sub>COOH</sub> materials, which can be attributed to the oxidation of copper during the preparation of both materials. In addition, the narrow and strong peaks of all samples indicate good crystallinity. The crystal sizes of CuFe<sub>2</sub>O<sub>4</sub>, CuFe<sub>2</sub>O<sub>4</sub>@SiO<sub>2</sub> and

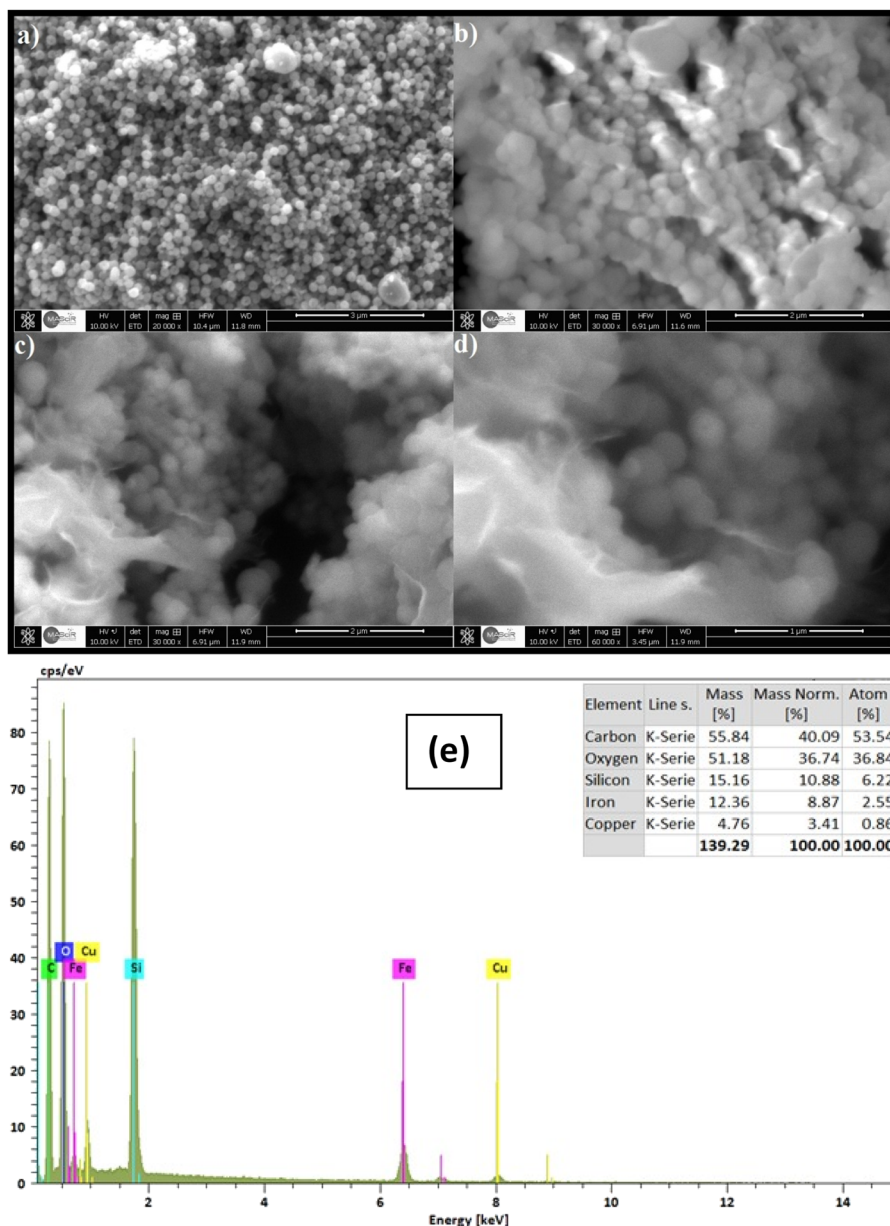


Fig. 3 SEM images of CuFe<sub>2</sub>O<sub>4</sub> (a), CuFe<sub>2</sub>O<sub>4</sub>@SiO<sub>2</sub> (b) CuFe<sub>2</sub>O<sub>4</sub>@SiO<sub>2</sub>-GO<sub>COOH</sub> (c and d) and EDX spectrum of CuFe<sub>2</sub>O<sub>4</sub>@SiO<sub>2</sub>-GO<sub>COOH</sub> (e).



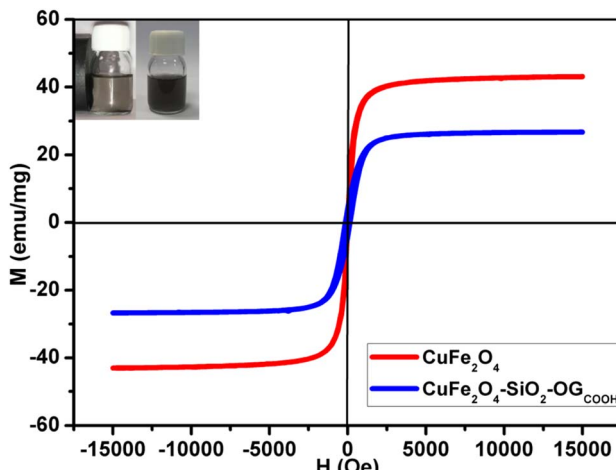


Fig. 4 Magnetization curves of  $\text{CuFe}_2\text{O}_4$  and  $\text{CuFe}_2\text{O}_4@\text{SiO}_2\text{-GO}_{\text{COOH}}$ . The inset shows the photographs of the separation processes of  $\text{CuFe}_2\text{O}_4@\text{SiO}_2\text{-GO}_{\text{COOH}}$  with external magnetic field.

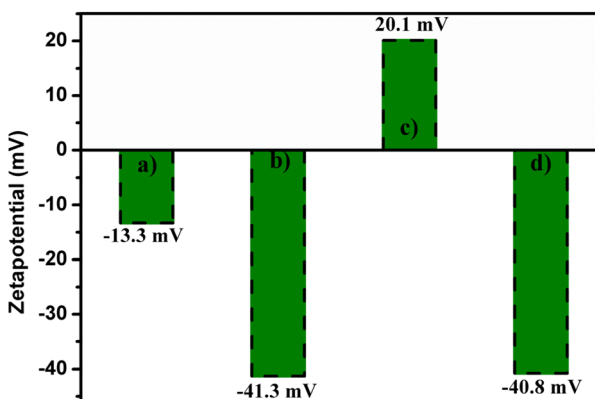


Fig. 5 Zeta potential of  $\text{CuFe}_2\text{O}_4$  (a),  $\text{CuFe}_2\text{O}_4@\text{SiO}_2$  (b),  $\text{CuFe}_2\text{O}_4@\text{SiO}_2\text{-NH}_2$  (c) and  $\text{CuFe}_2\text{O}_4@\text{SiO}_2\text{-GO}_{\text{COOH}}$  (d).

$\text{CuFe}_2\text{O}_4@\text{SiO}_2\text{-GO}_{\text{COOH}}$  were calculated based on the Scherrer equation and are 21.8, 22.4, and 19.8 nm, respectively (as shown in Table 1).

The structures and chemical species present in  $\text{CuFe}_2\text{O}_4$ ,  $\text{CuFe}_2\text{O}_4@\text{SiO}_2$  and  $\text{CuFe}_2\text{O}_4@\text{SiO}_2\text{-GO}_{\text{COOH}}$  were identified by FT-IR analysis. As depicted in Fig. 2, the broad peaks at  $3402$  and  $1620\text{ cm}^{-1}$  correspond to the hydroxyl ( $\text{OH}$ ) stretching vibrations caused by the presence of adsorbed water. The metal oxide stretching vibration peaks were observed at  $576\text{ cm}^{-1}$  for all samples. The characteristic peaks of silica were identified at  $1092$  and  $473\text{ cm}^{-1}$  for  $\text{CuFe}_2\text{O}_4@\text{SiO}_2$  and  $\text{CuFe}_2\text{O}_4@\text{SiO}_2\text{-GO}_{\text{COOH}}$ , confirming the presence of  $\text{SiO}_2$  coating on the surface of  $\text{CuFe}_2\text{O}_4$  materials. Furthermore, minor peaks in the range of  $2000\text{--}2800\text{ cm}^{-1}$  were observed for  $\text{CuFe}_2\text{O}_4@\text{SiO}_2$  and  $\text{CuFe}_2\text{O}_4@\text{SiO}_2\text{-GO}_{\text{COOH}}$ , which can be attributed to the C-H stretching vibration caused by the grafting of APTMS and GO.

The morphology of  $\text{CuFe}_2\text{O}_4$ ,  $\text{CuFe}_2\text{O}_4@\text{SiO}_2$  and  $\text{CuFe}_2\text{O}_4@\text{SiO}_2\text{-GO}_{\text{COOH}}$  samples was investigated by SEM analysis. As shown in Fig. 3a, the  $\text{CuFe}_2\text{O}_4$  nanoparticles are spherical, narrowly distributed, and uniform in shape and size. The SEM

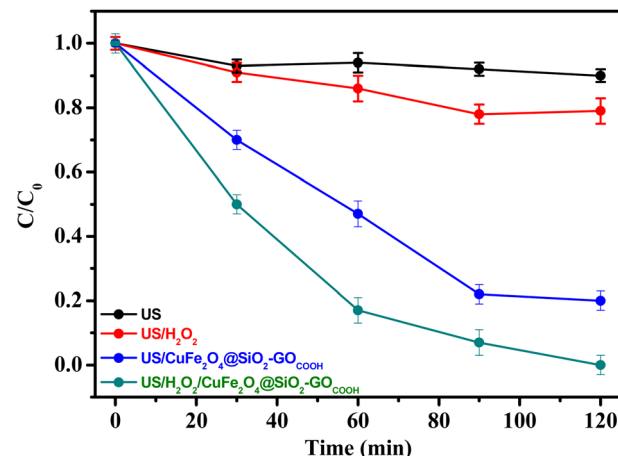


Fig. 6 Degradation efficiency ( $C/C_0$ ) of methidathion by various sonocatalytic systems. Reaction conditions: [methidathion] = 5 ppm,  $\text{H}_2\text{O}_2$  5%,  $T = 25\text{ }^\circ\text{C}$ .

image of  $\text{CuFe}_2\text{O}_4@\text{SiO}_2$  materials shown in Fig. 3b indicates that the  $\text{CuFe}_2\text{O}_4$  nanoparticles retain their morphological properties, except for a slight change in their shape and particle size. This result confirms that the silica groups were successfully coated on the surface of  $\text{CuFe}_2\text{O}_4$  nanoparticles, preventing the interaction and agglomeration of  $\text{CuFe}_2\text{O}_4$  magnetic nanoparticles. Furthermore, Fig. 3c and d show the presence of GO sheets in the  $\text{CuFe}_2\text{O}_4@\text{SiO}_2\text{-GO}_{\text{COOH}}$  nanoparticles, and we observed that the surface of  $\text{CuFe}_2\text{O}_4$  materials becomes smoother. Additionally, the element composition and distribution of  $\text{CuFe}_2\text{O}_4@\text{SiO}_2\text{-GO}_{\text{COOH}}$  were determined using energy-dispersive X-ray (EDX) analysis. As shown in Fig. 4, the EDX spectrum confirms the presence of copper, iron, silica, and oxygen.

The magnetic properties of  $\text{CuFe}_2\text{O}_4$ ,  $\text{CuFe}_2\text{O}_4@\text{SiO}_2\text{-GO}_{\text{COOH}}$  samples were determined using a SQUID magnetometer from  $\pm 15\,000$  Oe at room temperature. Fig. 4 shows the

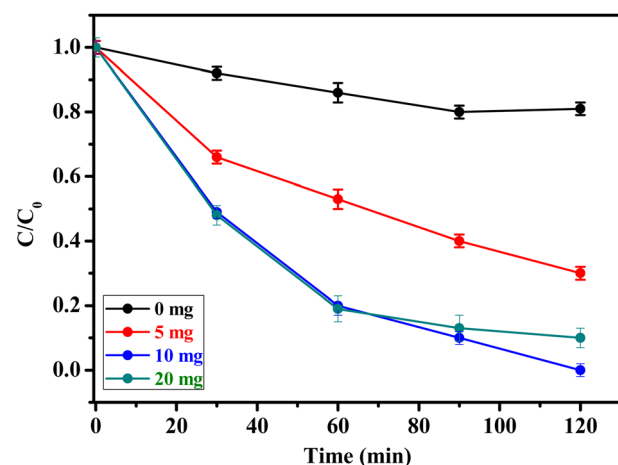


Fig. 7 Effect of amount of catalyst on methidathion degradation over  $\text{CuFe}_2\text{O}_4@\text{SiO}_2\text{-GO}_{\text{COOH}}$ . Reaction conditions: [methidathion] = 5 ppm,  $\text{H}_2\text{O}_2$  5%,  $T = 25\text{ }^\circ\text{C}$ .

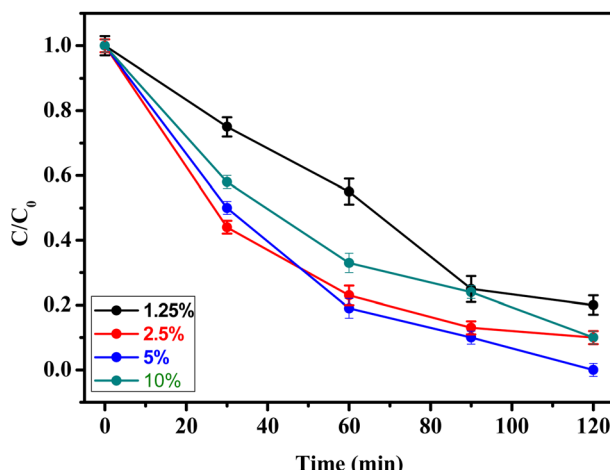


Fig. 8 Effect of  $\text{H}_2\text{O}_2$  on pesticide degradation over  $\text{CuFe}_2\text{O}_4@\text{SiO}_2\text{-GO}_{\text{COOH}}$ . Reaction conditions: [methidathion] = 5 ppm, amount of catalyst = 10 mg,  $T = 25^\circ\text{C}$ .

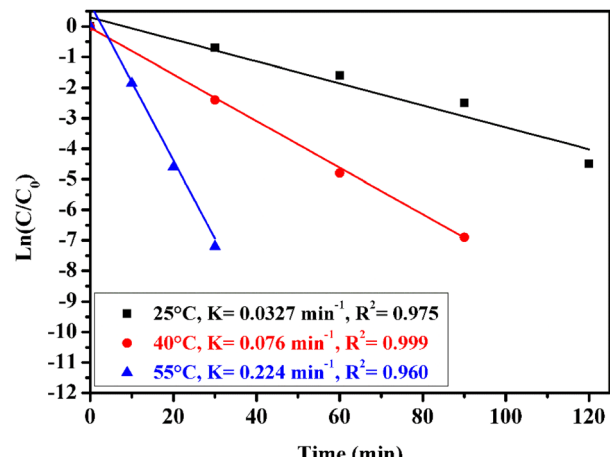


Fig. 9 Effect of reaction temperature on methidathion degradation over the  $\text{CuFe}_2\text{O}_4@\text{SiO}_2\text{-GO}_{\text{COOH}}$  sono-catalyst. Reaction conditions: [methidathion] = 5 ppm, catalyst amount = 10 mg and  $\text{H}_2\text{O}_2$  5%.

magnetic hysteresis loops of  $\text{CuFe}_2\text{O}_4$  and  $\text{CuFe}_2\text{O}_4@\text{SiO}_2\text{-GO}_{\text{COOH}}$ . The saturation magnetization ( $M_s$ ) value for  $\text{CuFe}_2\text{O}_4$  was 43.24 emu g<sup>-1</sup>. Compared to the  $M_s$  value of  $\text{CuFe}_2\text{O}_4$ ,  $\text{CuFe}_2\text{O}_4@\text{SiO}_2\text{-GO}_{\text{COOH}}$  had a lower value of 26.35 emu g<sup>-1</sup>, which can be explained by the surface coating of  $\text{CuFe}_2\text{O}_4$  magnetic particles with  $\text{SiO}_2$ . The magnetization curves of  $\text{CuFe}_2\text{O}_4$  and  $\text{CuFe}_2\text{O}_4@\text{SiO}_2\text{-GO}_{\text{COOH}}$  show negligible remanence ( $M_r$ ) and coercivity ( $H_c$ ), indicating superparamagnetic behavior of both materials. Additionally, the  $\text{CuFe}_2\text{O}_4@\text{SiO}_2\text{-GO}_{\text{COOH}}$  materials can be dispersed in deionized water to form a black solution before magnetic separation (as shown in the inserted Fig. 4). By applying an external magnetic field, the  $\text{CuFe}_2\text{O}_4@\text{SiO}_2\text{-GO}_{\text{COOH}}$  sample can be easily separated, and the solution becomes colorless.

The surface charge of all samples was investigated using zeta potential measurements. To prepare the samples, all materials were dispersed in deionized water to form a homogeneous

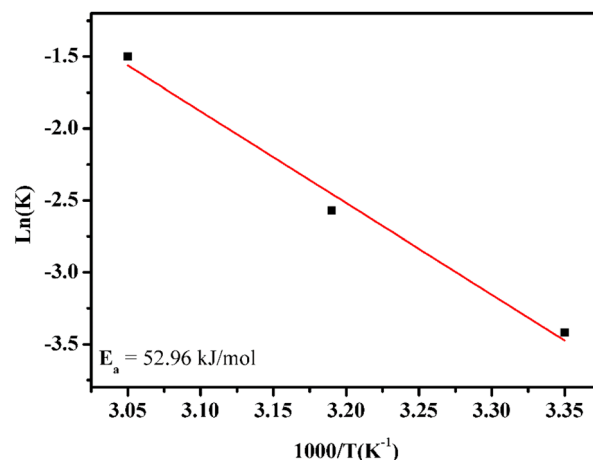


Fig. 10 Arrhenius plot with linear regression. Reaction conditions: [methidathion] = 5 ppm, catalyst amount = 10 mg and  $\text{H}_2\text{O}_2$  5%.

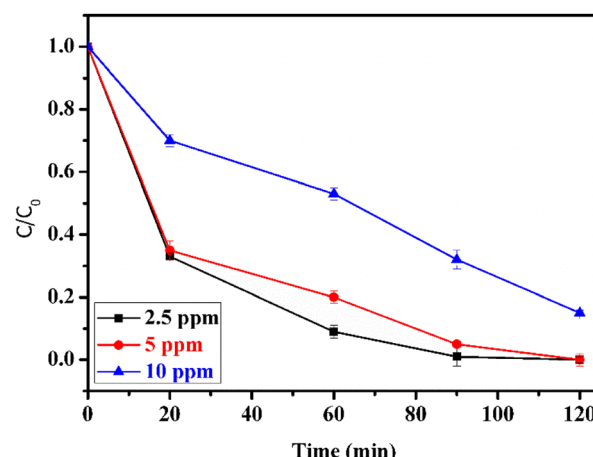


Fig. 11 Effect of methidathion concentration. Reaction conditions:  $\text{H}_2\text{O}_2$  5%, catalyst amount = 10 mg.

solution. As shown in Fig. 5, the zeta potentials of  $\text{CuFe}_2\text{O}_4$  and  $\text{CuFe}_2\text{O}_4@\text{SiO}_2$  were -13.3 and -41.3 mV, respectively, indicating that the surface of both materials was negatively charged. After amine functionalization of  $\text{CuFe}_2\text{O}_4@\text{SiO}_2$ , the surface charge became positive due to the presence of  $\text{NH}_2$  groups on the material's surface.<sup>50</sup> Subsequently,  $\text{CuFe}_2\text{O}_4@\text{SiO}_2\text{-NH}_2$  nanoparticles immobilized on GO showed a zeta potential value of -40.8 mV, indicating that the surface of  $\text{CuFe}_2\text{O}_4@\text{SiO}_2\text{-GO}_{\text{COOH}}$  was negatively charged due to the formation of covalent bonding between the carboxylic groups of GO and amine groups. These results suggest that the  $\text{CuFe}_2\text{O}_4@\text{SiO}_2\text{-GO}_{\text{COOH}}$  material could be used as a potential adsorbent for the removal of negatively charged pollutants.

The performance of  $\text{CuFe}_2\text{O}_4@\text{SiO}_2\text{-GO}_{\text{COOH}}$  as a sonocatalyst for methidathion degradation was evaluated. Fig. 6 shows the concentration of methidathion degradation ( $C_t/C_0$ ) as a function of reaction time using various sonocatalytic systems. Firstly, it can be observed that ultrasonic irradiations alone had no significant effect on the degradation of methidathion. Slight



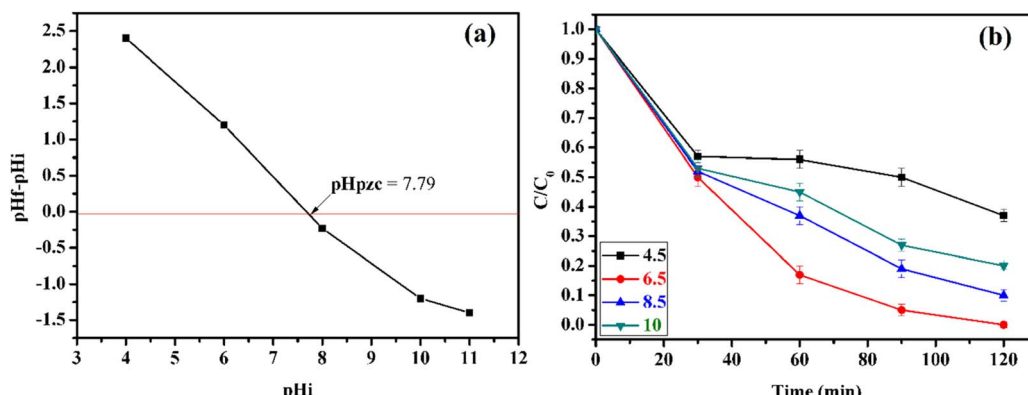


Fig. 12 Charge surface of the  $\text{CuFe}_2\text{O}_4@\text{SiO}_2\text{-GO}_{\text{COOH}}$  sonocatalyst at different pH (a) and effect of pH on methidathion degradation over the  $\text{CuFe}_2\text{O}_4@\text{SiO}_2\text{-GO}_{\text{COOH}}$  sonocatalyst (b). Reaction conditions: [methidathion] = 5 ppm, catalyst amount = 10 mg and  $\text{H}_2\text{O}_2$  5%.

increase in the degradation of methidathion was observed when using both  $\text{H}_2\text{O}_2$  as an oxidizing agent and ultrasonic irradiations. However, when combined with  $\text{CuFe}_2\text{O}_4@\text{SiO}_2\text{-GO}_{\text{COOH}}$  as a sonocatalyst, ultrasonic irradiations had a significant effect on the degradation of methidathion. The highest degradation of methidathion was achieved when ultrasound irradiations,  $\text{H}_2\text{O}_2$ , and  $\text{CuFe}_2\text{O}_4@\text{SiO}_2\text{-GO}_{\text{COOH}}$  were combined as sonocatalyst. This result can be explained by the high concentration of hydroxyl radicals formed, leading to great degradation efficiency.<sup>51,52</sup>

The influence of catalyst concentration on the degradation rate of methidathion was investigated by using different concentrations of  $\text{CuFe}_2\text{O}_4@\text{SiO}_2\text{-GO}_{\text{COOH}}$  sonocatalyst. The results of this study are presented in Fig. 7. Firstly, it should be noted that the reaction in the absence of the catalyst gave a low degradation rate of methidathion. Increasing the amount of the catalyst from 5 to 10 mg led to an increase in the degradation rate of methidathion. However, increasing the amount of the catalyst beyond 10 mg did not result in an increase in the degradation rate of methidathion. Therefore, we have chosen 10 mg as the optimum amount of the catalyst for methidathion degradation.

The concentration of  $\text{H}_2\text{O}_2$  is important factors influencing the rate degradation of pesticide. In order, different concentrations of  $\text{H}_2\text{O}_2$  were evaluated in the rate degradation of methidathion. As can be shown in the Fig. 8, the rate degradation of methidathion increase with increasing the concentration of  $\text{H}_2\text{O}_2$  from 1.25 to 5%, respectively. This result can be explain by the formation of high concentration of  $\cdot\text{OH}$  radicals responsible for the degradation of methidathion.<sup>53</sup> However, increasing the  $\text{H}_2\text{O}_2$  concentration to 10% leads to decrease the rate degradation of methidathion due to the hydroxyl radical ( $\cdot\text{OH}$ ) scavenging effect.<sup>54</sup> Finally, the concentration of 5% was chosen as the optimum for the degradation of methidathion.

The influence of temperature on the degradation of methidathion over  $\text{CuFe}_2\text{O}_4@\text{SiO}_2\text{-GO}_{\text{COOH}}$  sonocatalyst was investigated at various temperatures. The results of this study are presented in Fig. 9. The kinetic constants were calculated from the plot of  $\ln(C_0/C_t)$  versus time, and it was observed that the degradation of methidathion over  $\text{CuFe}_2\text{O}_4@\text{SiO}_2\text{-GO}_{\text{COOH}}$  sonocatalyst at all temperatures followed the pseudo-first-order kinetics:

$$\ln(C_0/C_t) = k_{\text{app}}t$$

where  $C_0$  is the initial concentration of methidathion,  $C_t$  is the methidathion concentration at time  $t$ , and  $k_{\text{app}}$  represents the pseudo-first order rate constant.

As shown in Fig. 9, when the temperature of the reaction was increased from 25 to 55 °C, the rate constant increased from 0.032 to 0.224  $\text{min}^{-1}$ , respectively. This increase can be attributed to the high concentration of  $\cdot\text{OH}$  radicals formed at higher temperatures, which are responsible for the degradation of methidathion.

Thereafter, the activation energy was determined by using an Arrhenius plot. Fig. 10 shows the natural logarithm of the rate constant,  $\ln(k)$ , as a function of  $1000/T$  according to the Arrhenius equation:

$$\ln k = \ln A - E_a/RT$$

where  $k$  is the rate constant,  $R$  is the gas constant (8.314  $\text{J mol}^{-1} \text{K}^{-1}$ ),  $T$  is the absolute temperature,  $A$  is the pre-exponential factor, and  $E_a$  is the activation energy, which corresponds to the slope of the plotted line.

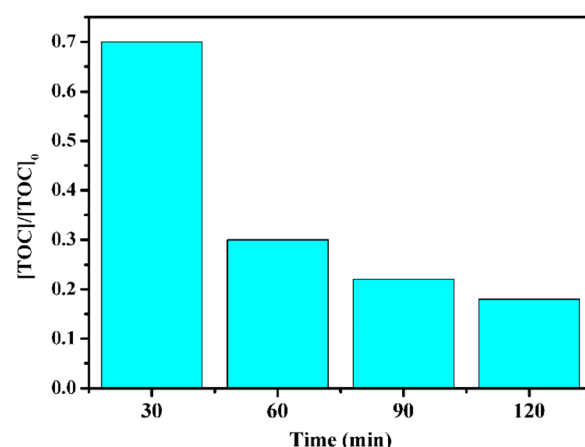


Fig. 13 TOC removal efficiency of methidathion using  $\text{CuFe}_2\text{O}_4@\text{-SiO}_2\text{-GO}_{\text{COOH}}$  as a catalyst. Reaction conditions: [pesticide] = 5 ppm, catalyst mount = 10 mg and  $\text{H}_2\text{O}_2$  5%.



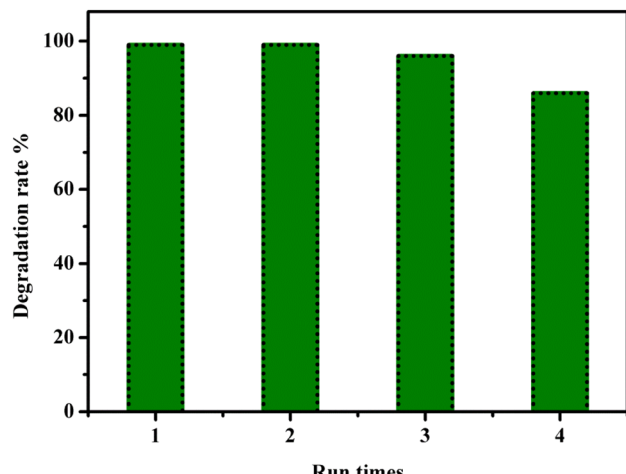


Fig. 14 Reuse performance of the  $\text{CuFe}_2\text{O}_4@\text{SiO}_2\text{-GO}_{\text{COOH}}$  catalyst in pesticide degradation. Reaction conditions: [pesticide] = 5 ppm, catalyst amount = 10 mg and  $\text{H}_2\text{O}_2$  5%.

The activation energy for methidathion degradation using  $\text{CuFe}_2\text{O}_4@\text{SiO}_2\text{-GO}_{\text{COOH}}$  as a sonocatalyst was found to be 52.96  $\text{kJ mol}^{-1}$ .

The initial concentration of methidathion plays an important role in the rate of degradation. To investigate this, different methidathion concentrations (2.5, 5, and 10 ppm) were used, and the rate of degradation was determined. As shown in Fig. 11, the rate of degradation remains constant when increasing the methidathion concentration from 2.5 to 5 ppm, but it decreases for 10 ppm methidathion concentration. This result can be explained by the decreasing number of active sites at higher methidathion concentrations due to their adsorption on the surface of the  $\text{CuFe}_2\text{O}_4@\text{SiO}_2\text{-GO}_{\text{COOH}}$  sonocatalyst.

The pH is a critical factor that influences the rate of degradation of methidathion, as it affects the adsorption/desorption of methidathion on the surface of the  $\text{CuFe}_2\text{O}_4@\text{SiO}_2\text{-GO}_{\text{COOH}}$  sonocatalyst. Firstly, the surface charge of  $\text{CuFe}_2\text{O}_4@\text{SiO}_2\text{-GO}_{\text{COOH}}$  sonocatalyst as a function of pH value was investigated. As shown in Fig. 12a, the surface charge of  $\text{CuFe}_2\text{O}_4@\text{SiO}_2\text{-GO}_{\text{COOH}}$  is negatively charged for a pH value lower than 7.79.

However, the surface charge of  $\text{CuFe}_2\text{O}_4@\text{SiO}_2\text{-GO}_{\text{COOH}}$  becomes positive for a pH value higher than 7.79. On the other hand, to study the effect of pH on methidathion degradation, the pH of the solution was adjusted to the desired value by adding NaOH (0.1 M) and HCl (0.1 M). Different pH values were obtained and their effect on methidathion degradation was evaluated. According to Fig. 12b, it can be observed that the rate of methidathion degradation increases with increasing pH value from 4.5 to 6.5. However, increasing the pH value greater than 6.5 leads to a decrease in the rate of methidathion degradation. These results can be explained by the electrostatic interaction between the positive charge of  $\text{CuFe}_2\text{O}_4@\text{SiO}_2\text{-GO}_{\text{COOH}}$  sonocatalyst and the negative charge of methidathion at a pH lower than 7.79.

To further investigate methidathion degradation, we measured the total organic carbon (TOC) using the US/ $\text{CuFe}_2\text{O}_4@\text{SiO}_2\text{-GO}_{\text{COOH}}/\text{H}_2\text{O}_2$  system, which is widely used to evaluate the degree of mineralization of organic species. As shown in Fig. 13, the TOC removal efficiency of methidathion reached 90% after 120 minutes in the presence of the US/ $\text{CuFe}_2\text{O}_4@\text{SiO}_2\text{-GO}_{\text{COOH}}/\text{H}_2\text{O}_2$  system. This finding confirms that the as-prepared samples can mineralize methidathion to residual organic molecules.

The reusability of the catalyst is a crucial factor to consider for large-scale industrial usage. Therefore, we investigated the reusability of our sonocatalyst,  $\text{CuFe}_2\text{O}_4@\text{SiO}_2\text{-GO}_{\text{COOH}}$ . The sonocatalyst was easily separated using an external magnet and washed several times with water and dichloroethane to remove any organic traces. The recuperated sonocatalyst was then used as a recyclable sonocatalyst for the degradation of Methiadation in multiple runs. As shown in Fig. 14, the  $\text{CuFe}_2\text{O}_4@\text{SiO}_2\text{-GO}_{\text{COOH}}$  sonocatalyst could be used consecutively for the degradation of Methiadation with a slight decrease in performance after three runs. This decrease could be attributed to the deposition of organic matter on the surface of  $\text{CuFe}_2\text{O}_4@\text{SiO}_2\text{-GO}_{\text{COOH}}$  sonocatalyst, which blocks active sites and reduces the effectiveness of the catalyst in a catalyzed reaction. In addition, the  $\text{CuFe}_2\text{O}_4@\text{SiO}_2\text{-GO}_{\text{COOH}}$  exhibits superior or comparable catalytic activity compared to most state-of-the-art highly active catalysts reported for pesticide degradation using  $\text{H}_2\text{O}_2$  as an oxidizing agent and ultrasonic irradiation (Table 2).

Table 2 Application of different catalysts for pesticide degradation by activating  $\text{H}_2\text{O}_2^a$

Sample	Pesticides	Catalyst dosage	Aiders	Oxidant	Time (min)	Removal efficiency (%)	Ref.
Sepiolite/ $\text{Fe}_3\text{O}_4$ $\text{Fe}_3\text{O}_4@\text{MOF-2}$	Diuron (30 mg $\text{L}^{-1}$ )	1 g $\text{L}^{-1}$	US	$\text{H}_2\text{O}_2$ (40 mM)	80	100	55
	Diazinon (30 mg $\text{L}^{-1}$ )	0.7 g $\text{L}^{-1}$		Persulfate (10 mmol $\text{L}^{-1}$ )	120	98	56
TiO <sub>2</sub> -Fe <sup>3+</sup>	Terbutylazine (5 mg $\text{L}^{-1}$ )	TiO <sub>2</sub> (1 g $\text{L}^{-1}$ ), Fe <sup>3+</sup> (34 mg $\text{L}^{-1}$ )	PC	$\text{H}_2\text{O}_2$ (1.32 mmol $\text{L}^{-1}$ )	20	100	57
Ag-TiO <sub>2</sub>	<i>p</i> -Chlorophenol (100 mg $\text{L}^{-1}$ )	1 g $\text{L}^{-1}$	US	$\text{H}_2\text{O}_2$ (450 mg $\text{L}^{-1}$ )		75	58
$\text{CuFe}_2\text{O}_4@\text{SiO}_2\text{-GO}_{\text{COOH}}$	Methidathion (5 mg $\text{L}^{-1}$ )	0.4 g $\text{L}^{-1}$	US	$\text{H}_2\text{O}_2$ (5%)	120	100	This work

<sup>a</sup> US: ultrasonic; PC: photocatalysis.



## 4. Conclusion

In this study, we synthesized and characterized  $\text{CuFe}_2\text{O}_4@\text{SiO}_2\text{-GO}_{\text{COOH}}$  using various techniques, including XRD, FTIR, SEM, TEM, and SQUID magnetometry. We utilized the synthesized  $\text{CuFe}_2\text{O}_4@\text{SiO}_2\text{-GO}_{\text{COOH}}$  as a sonocatalyst for the degradation of Methdation pesticide under ultrasound irradiation. Our results indicated that the rate of Methdation degradation was affected by several reaction parameters, including pH, Methdation concentration, and the amount of  $\text{CuFe}_2\text{O}_4@\text{SiO}_2\text{-GO}_{\text{COOH}}$  sonocatalyst. The optimal conditions for Methdation degradation were found to be at pH 6.5, with 10 mg of  $\text{CuFe}_2\text{O}_4@\text{SiO}_2\text{-GO}_{\text{COOH}}$  sonocatalyst, and 5 ppm Methdation concentration. Notably,  $\text{CuFe}_2\text{O}_4@\text{SiO}_2\text{-GO}_{\text{COOH}}$  sonocatalyst could be easily separated using an external magnet, without the need for traditional separation and purification methods, aligning with green and sustainable chemistry principles. Furthermore, the sonocatalyst demonstrated reusability for up to four cycles, with only a slight decrease in its sonocatalytic activity for the degradation of Methdation pesticides. Our findings suggest that  $\text{CuFe}_2\text{O}_4@\text{SiO}_2\text{-GO}_{\text{COOH}}$  sonocatalyst can be a promising candidate for industrial application in the removal of Methdation pesticide from contaminated environments.

## Conflicts of interest

The authors declare that there is no conflict of interests regarding the publication of this paper.

## Acknowledgements

We are thankful Moroccan Foundation for Advanced Science, Innovation and Research (MAScIR) for the financial assistance towards this research.

## References

- 1 C. Wilson and C. Tisdell, *Ecol. Econ.*, 2001, **39**, 449–462.
- 2 J. Popp, K. Pető and J. Nagy, *Agron. Sustainable Dev.*, 2013, **33**, 243–255.
- 3 K.-H. Kim, E. Kabir and S. A. Jahan, *Sci. Total Environ.*, 2017, **575**, 525–535.
- 4 C. A. Damalas, *SRE*, 2009, **4**, 945–949.
- 5 C. A. Damalas and I. G. Eleftherohorinos, *Int. J. Environ. Res. Public Health*, 2011, **8**, 1402–1419.
- 6 A. Amaral, *Front. Public Health*, 2014, **2**, 6.
- 7 P. D. Stivaktakis, M. P. Kavvalakis, M. N. Tzatzarakis, A. K. Alegakis, M. N. Panagiotakis, P. Fragkiadaki, E. Vakonaki, E. Ozcagli, W. A. Hayes, V. N. Rakitskii and A. M. Tsatsakis, *Chemosphere*, 2016, **149**, 108–113.
- 8 S. E. Anderson and B. J. Meade, *Environ. Health Insights*, 2014, **8**, 51–62.
- 9 W. Aktar, D. Sengupta and A. Chowdhury, *Interdiscip. Toxicol.*, 2009, **2**, 1–12.
- 10 S. Bulut, S. F. Erdoganmus, M. Konuk and M. Cemek, *Ekoloji*, 2010, **19**, 24–31.
- 11 S. Piel, E. Baurès and O. Thomas, *Int. J. Environ. Res. Public Health*, 2012, **9**, 4433–4451.
- 12 K. Narita, Y. Matsui, K. Iwao, M. Kamata, T. Matsushita and N. Shirasaki, *Environ. Int.*, 2014, **63**, 114–120.
- 13 J. E. Barbash, G. P. Thelin, D. W. Kolpin and R. J. Gilliom, *J. Environ. Qual.*, 2001, **30**, 831–845.
- 14 K. F. Mendes, A. P. J. Régo, V. Takeshita and V. L. Tornisielo, in *Organic Pollutants*, IntechOpen, 2019.
- 15 P. A. Shivajirao, *Int. J. Adv. Eng. Res. Stud.*, 2012, 275–283.
- 16 N. Matsumoto, H. Uemoto and H. Saiki, *Water Res.*, 2007, **41**, 2541–2550.
- 17 J. Wang and C. Chen, *Biotechnol. Adv.*, 2009, **27**, 195–226.
- 18 L. Chai, Q. Li, Q. Wang and X. Yan, *Environ. Sci. Pollut. Res. Int.*, 2018, **25**, 17250–17267.
- 19 S. Mohamed, *Wastewater Treatment Engineering*, 2015.
- 20 J. Gomes, E. Domingues, M. Gmurek, R. M. Quinta-Ferreira and R. C. Martins, *Energy Rep.*, 2020, **6**, 666–671.
- 21 C. Amor, L. Marchão, M. S. Lucas and J. A. Peres, *Water*, 2019, **11**, 205.
- 22 P. R. Gogate and A. B. Pandit, *Adv. Environ. Res.*, 2004, **8**, 501–551.
- 23 S. Gligorovski, R. Strekowski, S. Barbat and D. Vione, *Chem. Rev.*, 2015, **115**, 13051–13092.
- 24 M. A. Oturan and J.-J. Aaron, *Crit. Rev. Environ. Sci. Technol.*, 2014, **44**, 2577–2641.
- 25 Y. Guo, X. Mi, G. Li and X. Chen, *J. Chem.*, 2017, **2017**, 2830138.
- 26 A. A. Pradhan and P. R. Gogate, *J. Hazard. Mater.*, 2010, **173**, 517–522.
- 27 M. T. Taghizadeh and A. Mehrdad, *Ultrason. Sonochem.*, 2003, **10**, 309–313.
- 28 H. Liu, M. Y. Liang, C. S. Liu, Y. X. Gao and J. M. Zhou, *Chem. Eng. J.*, 2009, **153**, 131–137.
- 29 C. Minero, M. Lucchiari, D. Vione and V. Maurino, *Environ. Sci. Technol.*, 2005, **39**, 8936–8942.
- 30 H. A. Oualid, O. Amadine, Y. Essamlali, I. M. Kadmiri, H. E. Arroussi and M. Zahouily, *Nanoscale Adv.*, 2019, **1**, 3151–3163.
- 31 M. Pirsahab and N. Moradi, *RSC Adv.*, 2020, **10**, 7396–7423.
- 32 P. Gholami, L. Dinpazhoh, A. Khataee and Y. Orooji, *Ultrason. Sonochem.*, 2019, **55**, 44–56.
- 33 J. Wang, Z. Jiang, L. Zhang, P. Kang, Y. Xie, Y. Lv, R. Xu and X. Zhang, *Ultrason. Sonochem.*, 2009, **16**, 225–231.
- 34 J. Wang, Y. Lv, L. Zhang, B. Liu, R. Jiang, G. Han, R. Xu and X. Zhang, *Ultrason. Sonochem.*, 2010, **17**, 642–648.
- 35 J. Hartmann, P. Bartels, U. Mau, M. Witter, W. V. Tümping, J. Hofmann and E. Nietzschmann, *Chemosphere*, 2008, **70**, 453–461.
- 36 N. B. Bokhale, S. D. Bomble, R. R. Dalbhanjan, D. D. Mahale, S. P. Hinge, B. S. Banerjee, A. V. Mohod and P. R. Gogate, *Ultrason. Sonochem.*, 2014, **21**, 1797–1804.
- 37 A. M. Abu-Dief and S. M. Abdel-Fatah, *Beni-Suef University J. Basic Appl. Sci.*, 2018, **7**, 55–67.
- 38 S. Kameoka, T. Tanabe and A. P. Tsai, *Catal. Lett.*, 2005, **100**, 89–93.
- 39 L. S. Mdletshe, P. R. Makgwane and S. S. Ray, *Nanomaterials*, 2019, **9**, 1140.



40 J. Plocek, A. Hutlová, D. Niž and J. Buršík, *Mater. Sci.*, 2005, **23**, 697–705.

41 F. Liu, F. Niu, N. Peng, Y. Su and Y. Yang, *RSC Adv.*, 2015, **5**, 18128–18136.

42 E. Aslani, A. Abri and M. Pazhang, *Colloids Surf., B*, 2018, **170**, 553–562.

43 R. Dhandha and M. Kidwai, *RSC Adv.*, 2016, **6**, 53430–53437.

44 R. Tabit, O. Amadine, Y. Essamlali, K. Dâoun, A. Rhihil and M. Zahouily, *RSC Adv.*, 2018, **8**, 1351–1360.

45 Y. Zhang, Q. Zhu, Y. Zhao, X. Yang and L. Jiang, *Chin. J. Chem. Phys.*, 2023, DOI: [10.1063/1674-0068/cjcp2210150](https://doi.org/10.1063/1674-0068/cjcp2210150).

46 F. Liu, F. Niu, N. Peng, Y. Su and Y. Yang, *RSC Adv.*, 2015, **5**, 18128–18136.

47 W. S. Hummers and R. E. Offeman, *J. Am. Chem. Soc.*, 1958, **80**, 1339.

48 K. Ali, A. Bahadur, A. Jabbar, S. Iqbal, I. Ahmad and M. I. Bashir, *J. Magn. Magn. Mater.*, 2017, **434**, 30–36.

49 J. Zheng, Z. Lin, W. Liu, L. Wang, S. Zhao, H. Yang and L. Zhang, *J. Mater. Chem. B*, 2014, **2**, 6207–6214.

50 Y. Li, L. Yang, X. Liu, N. Li, L. Zhang, Q. Li, Y. Yang, Y. Duan and F. Zhang, *J. Mater. Sci.*, 2015, **50**, 5960–5969.

51 M. Sayed, L. A. Shah, J. A. Khan, N. S. Shah, H. M. Khan, R. A. Khan, A. R. Khan and A. M. Khan, *J. Chil. Chem. Soc.*, 2016, **61**, 2949–2953.

52 G. Lyngsie, L. Krumina, A. Tunlid and P. Persson, *Sci. Rep.*, 2018, **8**, 1–9.

53 M. Xing, W. Xu, C. Dong, Y. Bai, J. Zeng, Y. Zhou, J. Zhang and Y. Yin, *Chem.*, 2018, **4**, 1359–1372.

54 C. D. Fernando and P. Soysa, *MethodsX*, 2015, **2**, 283–291.

55 K. Hou, G. Wang, Y. Zhu, N. Ezzatahmadi, L. Fu, A. Tang, H. Yang and Y. Xi, *Appl. Clay Sci.*, 2019, **181**, 105243.

56 S. Sajjadi, A. Khataee, N. Bagheri, M. Koby, A. Şenocak, E. Demirbas and A. G. Karaoglu, *J. Ind. Eng. Chem.*, 2019, **77**, 280–290.

57 J. Tang, Y. Chen and Z. Dong, *J. Environ. Sci.*, 2019, **79**, 153–160.

58 S. K. Nandwani, A. K. Mungray and M. Chakraborty, *Indian J. Chem. Technol.*, 2015, **22**, 73–77.

